An investigation of pore water pressure and consolidation phenomenon in the unfrozen zone during soil freezing

Lianhai Zhang [a,b], Wei Ma [a,*], Chengsong Yang [a], Zhi Wen [a], Sheng Dong [c]

[a] State Key Laboratory of Frozen Soil Engineering, Cold and Arid Regions Environmental and Engineering Research Institute, Chinese Academy of Sciences, Lanzhou 730000, China
[b] University of Chinese Academy of Sciences, Beijing 100049, China
[c] College of Civil Engineering, Beijing University of Technology, Beijing 100049, China

ARTICLE INFO

ABSTRACT

Accurate modeling of soil deformation depends on the consideration of both frost heave deformation in the frozen zone and consolidation deformation in the unfrozen zone. Pore water pressure investigations are important for revealing these two deformation behaviors. Herein, we aim to reveal the consolidation process by measuring and analyzing changes in pore water pressure in the unfrozen zone. Using a custom-made pore water pressure gauge, we performed a series of real-time pore water pressure measurements in the unfrozen zone of silty clay and sandy soil samples that were exposed to closed and open freezing systems. The results show that the pore water pressure in the unfrozen zone generally increases at first and then decreases. The temperature changes in the unfrozen zone have no significant influence on the changes in pore water pressure, and the variations of the pore water pressure are mainly controlled by the stress and hydraulic boundary (changes in pore water pressure) conditions at the freezing front. Furthermore, changes in the pore water pressure are affected by several parameters, including soil type, water supply condition, initial moisture content, measured soil layer depth, and hydraulic conductivity. Soil consolidation is mainly caused by change in effective stress, which results from increase in total stress or decrease in pore pressure. Based on the observed pore water pressure variations and its numerical simulations, we propose that consolidation in the unfrozen zone during soil freezing includes compression-induced consolidation, which results from an increase in frost heaving stress, and vacuum-induced consolidation, which results from a decrease in pore water pressure. Each consolidation pattern plays an important role in the different stages of soil freezing. Compression-induced consolidation primarily occurs during the early stage of soil freezing, while vacuum-induced consolidation mainly occurs during the later stage of soil freezing.

© 2016 Elsevier B.V. All rights reserved.

1. Introduction

Investigation of the pore water pressure during soil freezing is essential when exploring the mechanisms of frost heave, which involves several problems, including the driving force of water migration, the mechanisms of ice segregation, accurate frost heave modeling, and the validity of the Clausius-Clapeyron equation (Ma et al., 2015). Therefore, it is important for geotechnical scientists and engineers to directly measure pore water pressure during experimental testing. However, methods for measuring pore water pressure during soil freezing have always been challenging (Zhang et al., 2013, 2014, 2015). Therefore, further development of frost heave theory has encountered a research bottleneck.

When considering soil deformation, soil samples that have been subjected to unidirectional freezing are generally divided into three zones: the frozen zone, the frozen fringe and the unfrozen zone. The soil in the frozen zone experiences a frost heaving process throughout the freezing process, while the soil in the unfrozen zone may experience a consolidation process. Research has indicated that consolidation of the unfrozen zone is accompanied by the migration of water from the unfrozen zone to the frozen fringe and frozen zones, but the relationship between the two processes remains unclear. Many studies have focused on frost heave phenomenon in the frozen zone. However, few studies have focused on consolidation phenomenon in the unfrozen zone. Consolidation behavior in the unfrozen zone is closely related to changes in pore water pressure and directly influences the accuracy of models for predicting the surface deformation of soils subjected to freezing and thawing. Therefore, as part of a series of studies, this paper mainly focuses on variations in pore water pressure and consolidation phenomenon in the unfrozen zone during soil freezing.

Although the significance of consolidation in the unfrozen zone of freezing soils has been widely acknowledged, most studies have been based on theoretical speculations and have lacked supporting pore

* Corresponding author.
  E-mail addresses: zhanglh@lzb.ac.cn (L. Zhang), mawei@lzb.ac.cn (W. Ma).

water pressure data due to the constraints of directly measuring pore water pressure. Consequently, little progress has been made in this field. Chamberlain and Gow (1979) speculated that the high consolidation of thawed sub-sea permafrost is attributed to decrease in the pore water pressure and increase in the effective stress during ground freezing. Chamberlain (1981) noted that the amount of consolidation in the unfrozen zone beneath the freezing front is likely related to the plastic limit, which is equal to the minimum soil moisture content during freezing and thawing process. Tiedje and Guo (2011) found that growth of ice lenses results in substantial decreases in pore pressure and ultimately dewatering and unsaturation in the unfrozen zone during closed-system tests without an external water supply. Consequently, it is important to determine consolidation behavior by directly measuring the pore water pressures within the unfrozen zone.

Moreover, experimental results showed that some water is often extruded from the unfrozen zone during the early stage of soil freezing (Arenson et al., 2005; Mcroberts and Morgenstern, 1975; Nakano, 1999), especially when the soil sample was tested under an external load (Loch, 1978a, 1978b; O'Neil and Miller, 1985). The water expulsion phenomenon implied that pore water pressure increases in the unfrozen zone. Large increase in frost heaving stress was observed during soil freezing (Penner, 1970; Takashi et al., 1981), which may greatly affect the pore water pressure and consolidation in the unfrozen zone. However, this topic has not been sufficiently studied. Most frost heave models, including the hydrodynamic model (Bronfenbrener, 2013; Harlan, 1973; Watanabe, 2008), segregation potential theory (Konrad and Morgenstem, 1980, 1981), and rigid ice model (Miller, 1978; O'neill, 1983; O'Neil and Miller, 1985), have always ignored consolidation in the unfrozen zone to simplify calculations. Although some studies noted consolidation phenomena in the unfrozen zone (Thomas et al., 2009; Zhou and Li, 2012), none had studied the impacts of frost heaving stress on consolidation in the unfrozen zone.

To investigate consolidation in the unfrozen zone, custom-made pore water pressure gauges were used to measure the pore water pressures in the unfrozen zones of different soils under different water supply conditions (closed-system or open-system). A detailed analysis was conducted to the pore water pressure changes and consolidation phenomenon in the unfrozen zone, and then the changes in pore water pressure were further simulated. In addition, the effects of frost heaving stress on consolidation phenomenon were discussed. By clarifying the variations in the pore water pressure and consolidation phenomenon in the unfrozen zone, we expect to provide a reference for accurately modeling frost heave.

2. Pore water pressure measurements in the unfrozen zone

2.1. Materials and methods

2.1.1. Testing system and pore water pressure test method

Experiments were designed and conducted using the XT5405 freeze-thaw cycling test apparatus manufactured by Xutemp Temptech Co. Ltd. (Fig. 1). The box temperature can be controlled between −20 °C and 20 °C, and the temperatures of the top and bottom plates can be controlled between −30 °C and 30 °C with a precision of ±0.2 °C. A cylindrical Perspex cell with lateral thermal insulation was placed in the test machine box. Two columns of holes were drilled in the wall of the cylindrical Perspex cell. One column contained ten holes for installing the temperature probes at intervals of 10 mm, and the other column contained several holes for inserting the pore water pressure probes into the soil at different depths below the surface. Two different cylindrical Perspex cells with different hole arrangements were applied throughout the experiments. The specific hole and probe arrangements are shown in Fig. 2. The high-sensitivity temperature probes (with a precision of 0.05 °C and a valid temperature range of −30 °C–30 °C) were manufactured and calibrated by the State Key Laboratory of Frozen Soil Engineering (Liu et al., 2011). A displacement gauge was installed on the top plate to measure the vertical displacement of the soil sample. Soil freezing experiments with two different water supply conditions (closed and open systems) were conducted using the test system. The soil sample was frozen with no water supply (closed-system freezing) when the valve was closed. The soil sample was frozen with water supply (open-system freezing) when the valve was open. Water was supplied using a reservoir bottle that monitored changes in water volume in real time.

The experimental objective was to form a method for determining pore water pressure. Takagi (1980) proposed a conceptual model for

1. Displacement gauge   5. Box of freeze-thaw machine   9. Vent for alcohol circulating
2. Top plate   6. Pore water pressure gauges   10. Temperature probes
3. Cylindrical Perspex cell 7. Reservoir bottle   11. Cryostat
4. Soil Sample   8. Bottom plate   12. Switching valve
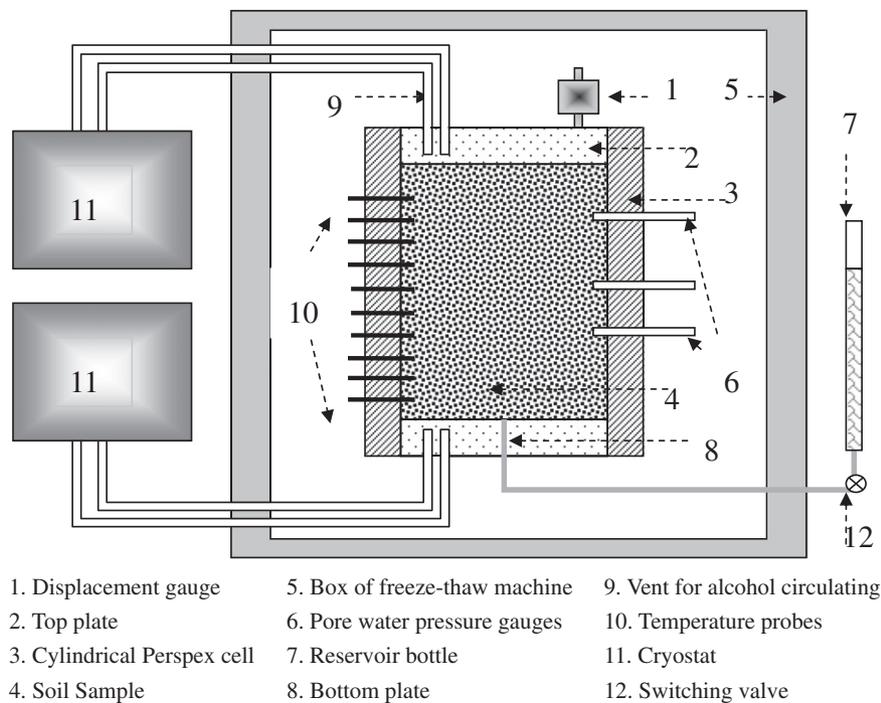
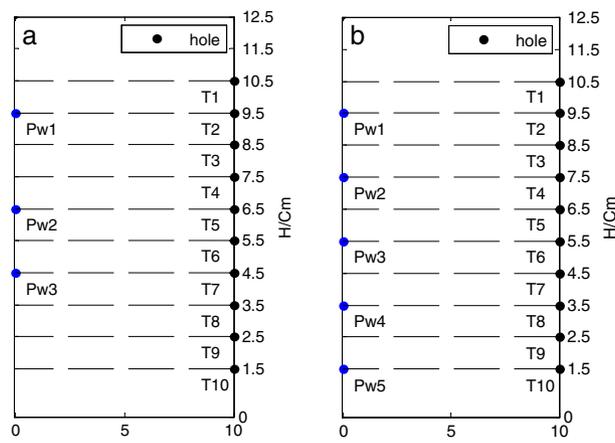Fig. 1. Sketch of the freeze-thaw testing system.

Fig. 2. Hole arrangements of two similar cylindrical Perspex cells.

measuring pore water pressure in which an ideal tensiometer was filled with pure water and placed in contact with the unfrozen film water through a semi-permeable membrane that allowed water to pass but not solutes. In this system, the pore water pressure was obtained when the pure water and film water achieve thermodynamic equilibrium. The main challenges when designing a pore water pressure gauge included choosing an appropriate semi-permeable membrane material and choosing a suitable medium for the tensiometer. In laboratory or field experiments on thawed soils, these issues were generally resolved because pure water was served as a transmission medium, and porous ceramic was served as a semi-permeable membrane material (Fukuda, 1983). However, the pure water in the tensiometer will freeze at sub-freezing temperatures and lose its transmission capability. Thus, a new medium is necessary as a substitute for pure water, and must meet two conditions. First, the medium must remain liquid at sub-freezing temperatures. Second, the new medium cannot pass through the semi-permeable membrane and enter the soil. Following considerable research efforts, ethyl alcohol (C_2H_6O) was selected as a new medium for use at sub-freezing temperatures (Mcgaw et al., 1983; Harris and Davies, 1998; Eigenbrod et al., 1996). Mcgaw et al. (1983) measured the pore water pressure during freezing using 10% ethyl alcohol. Eigenbrod et al. (1996) obtained the pore water pressure during freezing and thawing using 50% ethyl alcohol. However, Harris and Davies (1998) did not indicate the ethyl alcohol concentration used in their study.

Based on the results of these studies, we designed our pore water pressure gauge in three parts, as shown in Fig. 3. A small porous ceramic cup (approximately 5 mm in diameter) is joined to a pressure transducer via a plastic tube. The porous ceramic cup has a dual functionality, similar to that of a semi-permeable membrane, and allows water to pass freely while inhibiting the flow of alcohol into the soil sample to prevent disturbing the actual pore water pressure. Furthermore, alcohol can transmit the force as a highly effective medium at sub-freezing temperatures. Therefore, the plastic tube is filled with 99.7% ethyl alcohol (C_2H_6O) instead of pure water to permit pore water pressure measurements under freezing conditions. The pore water pressure can be ultimately acquired by using the pressure transducer, which has a
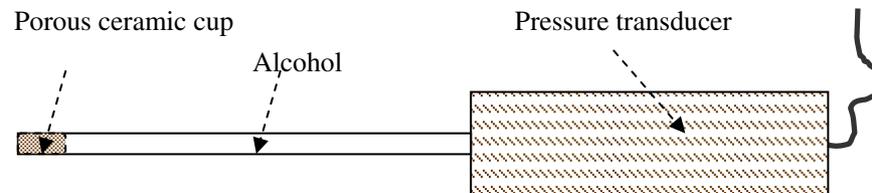
measuring range of −100 to 100 kPa with a reference pressure point (a standard atmospheric pressure) and an overall accuracy of ±0.1% FS (Full Scale).

2.1.2. Soil sample preparation and testing program

Two typical types of soil found along the Qinghai-Tibet railway were tested: a silty clay soil and a sandy soil. The grain size distributions and Atterberg limits of the soils are shown in Table 1. The soil samples were prepared and tested at the State Key Laboratory of Frozen Soil Engineering in Lanzhou, China. Five soil samples were prepared and measured during the experiments, a saturated sandy soil sample (SN1) and four silty clay soil samples (CN1, CN2, CN3, and CN4). Each soil sample was reconstituted by slurry mixing before being compressed into a cylindrical Perspex cell with an inner diameter of 101 mm. Other specific soil sample parameters, such as the initial moisture content and height, are shown in Table 2.

Based on water supply conditions, all experiments were divided into two groups. One group (SN1 and CN1) was tested under open–system freezing, and the other (CN2, CN3 and CN4) was tested under closed–system freezing. First, the cylindrical Perspex cell that was packed with the prepared soil sample was placed into a box of the freeze-thaw cycling test machine. Next, the sensors were installed, the temperature probes were inserted into the soil sample through the holes T1, T2, T3, T4, T5, T6, T7, T8, T9 and T10 shown in Fig. 2; the pore water pressure gauges were inserted into the soil sample through the holes PW1, PW2, PW3, PW4 and PW5 shown in Fig. 2; the displacement gauge was installed on the top plate, and the switching valve of the reservoir bottle was opened or closed according to the water supply condition during testing (Fig. 1). Finally, freezing experiments were conducted by controlling the top and bottom plate temperatures, as shown in Table 2. The CN2, CN3 and CN4 samples were subjected to two temperature conditions, constant temperature (stage I) and freezing (stage II), as shown in Table 2. During the constant temperature condition, each sample was kept at a temperature of 1.5 °C for approximately 15 h according to the box temperature of freeze-thaw cycling test apparatus. During soil freezing, each sample was frozen from the top down. However, samples SN1 and CN1 were only exposed to a freezing temperature condition, not subjected to the constant temperature condition, as shown in Table 2. Meanwhile, the pore water pressure, temperature and water volume absorbed into the soil sample were measured and recorded over ten-minute intervals during testing.

2.2. Experimental results

2.2.1. Influences of temperature on pore water pressure

Temperature changes from 22.5 °C to 1.5 °C did not result in apparent changes in the pore water pressure. The CN2, CN3 and CN4 samples were subjected to constant temperature prior to soil freezing (Table 2). The temperatures in the samples quickly decreased from approximately 22.5 °C to 1.5 °C, and the pore water pressures remained constant during this stage (stage I). For example, the pore water pressures of Pw3 and Pw4 in the CN2 sample remained constant (0 kPa) during the constant temperature period prior to freezing, as shown in Fig. 4. The results were because the positive temperatures of the whole sample did not result in ice-water phase change during the constant temperature stage, and thus the pore water pressures remained unchanged.

Fig. 3. Sketch of the pore water pressure probe.

Soil type	Hydraulic conductivity (cm/s)	Liquid limit	Plastic limit	Particle size (mm)						
				<0.075	0.075–0.1	0.1–0.25	0.25–0.5	0.5–1.0	1.0–2.0	>2.0
Sandy soil (%)	7.1×10^{-5}	/	/	21.3	46.8	21.7	6.2	3.7	0.3	0.0
Silty clay (%)	5.4×10^{-7}	25.5	11.9	19.8	51.9	17.5	7.4	2.9	0.5	0.0

However, the CN1 sample was not subjected to constant temperature prior to freezing (Table 2). In this case, the temperature in the unfrozen zone quickly decreased from approximately 22.5 °C to 1.5 °C, and the pore water pressure increased at first and then decreased, as shown in Fig. 5. In addition, when soil freezing began (stage II), the T6 and T8 temperatures of the CN2 sample slightly decreased and the Pw3 and Pw4 pore water pressures increased at first and then decreased, as shown in Fig. 4. These results were attributed to the influences of soil freezing in adjacent area (the frozen fringe) where ice-water phase change occurred due to sub-freezing temperature, and thus the pore water pressures changed with the influences of the ice-water phase change.

Based on the results, we concluded that the changes in pore water pressure were not related to changes in temperature over a range of positive temperatures because the positive temperature range did not result in ice-water phase change. The change in pore water pressure must be induced by other factors. To investigate these factors, we made a detailed comparison of the pore water pressures in the unfrozen zone of the SN1, CN1, CN2, CN3, and CN4 soil samples.

2.2.2. Influences of water supply conditions on pore water pressure

The CN1 and CN2 soil samples had similar initial moisture contents but different water supply conditions. The CN1 soil sample was tested under open-system freezing, and the CN2 soil sample was tested under closed-system freezing. Fig. 4 shows the variations of the pore water pressure and their temperatures at the same depths in the unfrozen zones of the CN1 and CN2 soil samples. It was noted from Fig. 4 that the pore water pressures in the unfrozen zone showed similar behavior under different water supply conditions (open-system and closed-system conditions). However, the magnitude of pore water pressure change under open-system conditions was smaller than that of the change under closed-system conditions, which implied that the water supply condition has influence on the changes in pore water pressure.

2.2.3. Influences of soil type on the pore water pressure

The same water supply conditions (open-system) were used when testing the SN1 saturated sandy soil sample and the CN1 silty clay soil sample. Fig. 5 illustrates the pore water pressure curves and their temperature curves in the unfrozen zones. As shown in Fig. 5, the changes in pore water pressures differed between the different soil types. For example, the Pw3 pore water pressure of the CN1 silty clay soil sample increased during the early stage of freezing and decreased during the later stage of freezing. However, the Pw3 pore water pressure of the SN1 sandy sample showed unchanged. The T7 temperatures in the SN1

sandy samples and the CN1 silty clay sample showed similar changes at the same positions. The T7 temperatures of the SN1 and CN1 samples decreased quickly from room temperature before stabilizing at some positive temperature. In addition, the T7 temperature of the SN1 sample was slightly greater than that of the CN1 sample after 24 h. However, the variations of the pore water pressure were not affected by the slight temperature difference because the changes in the pore water pressure were not correlated with the temperature changes in the positive temperature range. Therefore, the differences in the pore water pressures may result from a combination of two factors. First, the pore water pressure in the sandy soil sample has a faster dissipation rate than the pore water pressure in the silty clay sample due to the higher hydraulic conductivity of the sandy soil (Table 1). Second, the silty clay soil sample may have a more significant increase in frost heaving stress and a greater decrease in pore water pressure than the sandy soil at the freezing front, which is recognized in the experimental observations where ice segregation occurs in the silty clay but not in the sandy soil. Consequently, the pore water pressure in the unfrozen zone of the silty clay increased (during the early stage of freezing) and decreased (during the later stage of freezing) more than the sandy soil.

2.2.4. Influences of the initial moisture content on the pore water pressure

The same water supply condition (closed-system) and different initial moisture contents (Table 2) were used in the CN2, CN3 and CN4 silty clay soil sample experiments. Fig. 6 shows the variations of the pore water pressures in the unfrozen zone with different initial moisture contents. The initial moisture content significantly affected the variations of the pore water pressure in the unfrozen zone. During the early stage of freezing, the soil sample with a higher initial moisture content experienced a greater increase in pore water pressure. For example, the pore water pressure increased by 17 kPa in the CN2 experiment, by 7.5 kPa in the CN3 experiment, and by 2.5 kPa in the CN4 experiment. During the later stage of soil freezing, the frozen state become stable, and the soil sample with a lower initial moisture content have a smaller pore water pressure. For example, the pore water pressure stabilized at approximately −20 kPa in the CN2 experiment, −35 kPa in the CN3 experiment, and −50 kPa in the CN4 experiment. During the constant temperature stage (stage I) before soil freezing, the pore water pressure was closely correlated with the initial soil moisture content, and a lower initial moisture content resulted in a smaller pore water pressure. For example, before the CN2, CN3 and CN4 samples were frozen, the pore water pressures were approximately 0 kPa, −7.5 kPa, and −15 kPa, respectively.

| Samples	Cell	Moisture content	Height (cm)	Water supply condition	Temperature conditions (°C)			
					Constant temperature (stage I)	Soil freezing (stage II)		
					Box temperature	Box temperature	Top plate	Bottom plate
SN1	a in Fig. 2	22.10%	11.9	Open-system	No	1.5	−3.0	3.0
CN1	a in Fig. 2	37.65%	12.5	Open-system	No	1.5	−5.0	3.0
CN2	b in Fig. 2	35.00%	13.3	Closed-system	1.5	1.0	−8.0	3.0
CN3	b in Fig. 2	26.52%	13.3	Closed-system	1.5	1.0	−8.0	3.0
CN4	b in Fig. 2	19.56%	13.3	Closed-system	1.5	1.0	−8.0	3.0
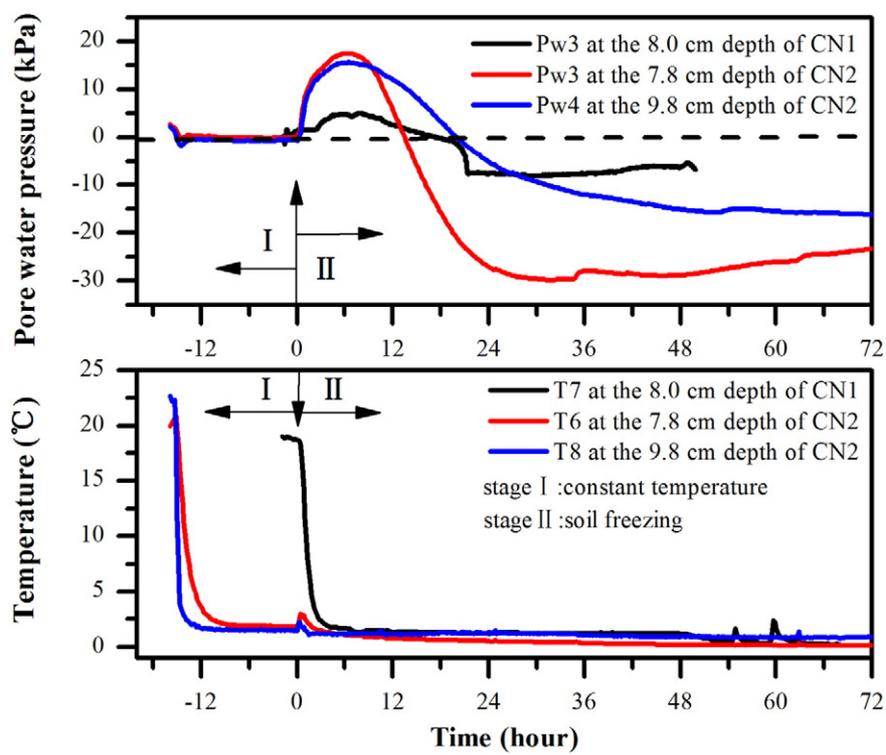
Fig. 4. Variations of the pore water pressure in the unfrozen zone of silty clay soil samples with different water supply conditions, soil sample CN1 with an open-system condition and CN2 with a closed-system condition.

2.2.5. Influences of depth on the pore water pressure

The Pw3 and Pw4 pore water pressure probes were located at different soil depths during freezing of the CN2 soil sample, as shown in Fig. 2. The Pw3 and Pw4 pore water pressures increased at similar magnitudes during the early stage of freezing and dissipated at different rates during the later stage of freezing, as shown in Fig. 7. The dissipation of the pore water pressure resulted from the migration of water from the unfrozen to the frozen zone. More soil suction occurred near the freezing front, and water was absorbed to the zone above the freezing front and served as a water source for ice segregation. Therefore, more rapid dissipation of the pore water pressure occurred near the freezing front, and the dissipation of the pore water pressure proceeded from the top to bottom.
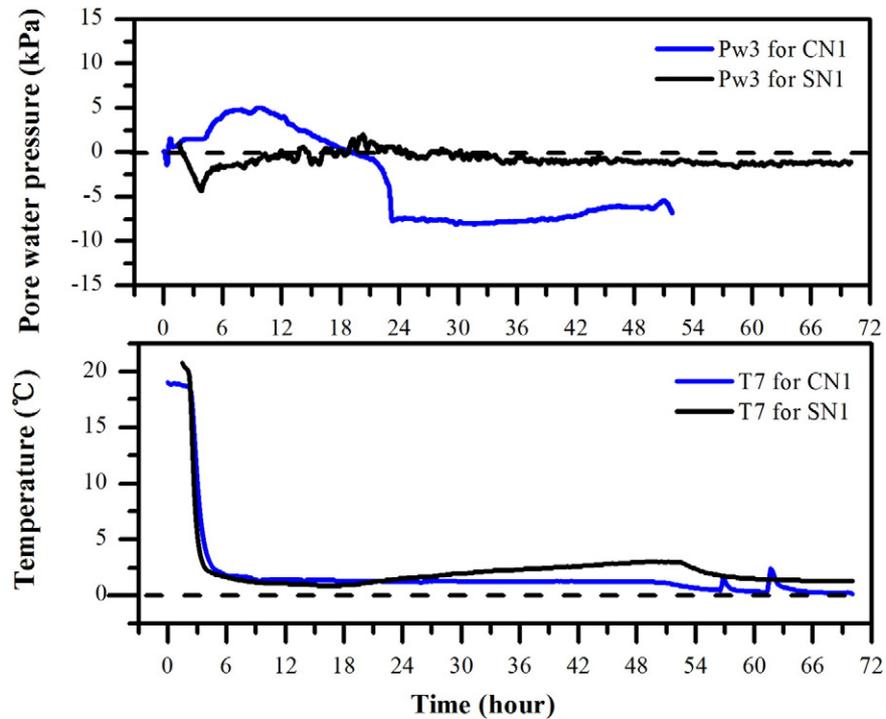

Fig. 5. Variations of pore water pressure in the unfrozen zone of the sandy soil sample SN1 and the silty clay sample CN1.
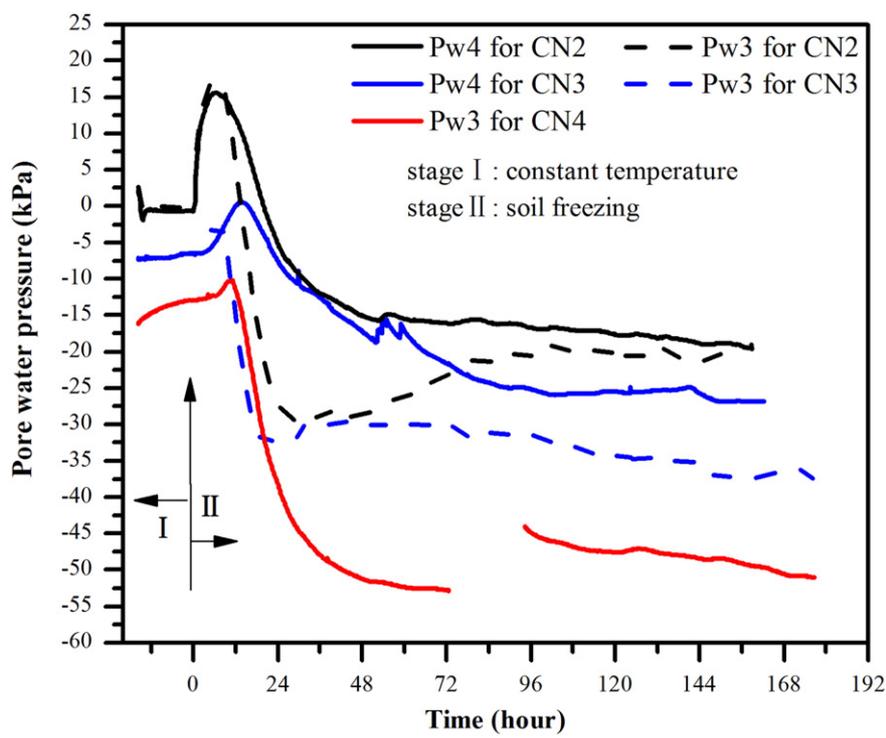
Fig. 6. Pore water pressure variations in the unfrozen zone with different initial moisture contents.

For example, the dissipation of the Pw3 pore water pressure occurred earlier and faster than that of the Pw4 pore water pressure.

2.3. Analysis of the results

Generally, soil consolidation is affected by boundary conditions. In freezing soils, changes in pore water pressure and consolidation in the unfrozen zone are largely controlled by the hydraulic and stress boundary conditions at the freezing front. Stress boundary conditions of the unfrozen zone are generally affected by external loading, unit weight of soil and the frost heaving stress of the frozen fringe. The frost heaving stress in the frozen fringe as a stress boundary condition has soil-compacting effects on the unfrozen zone during freezing. In addition, the stress induced by the unit weight of the soil is usually negligible. Thus, when experiment is conducted with no external load, increase in pore water pressure is mainly linked to increase in frost
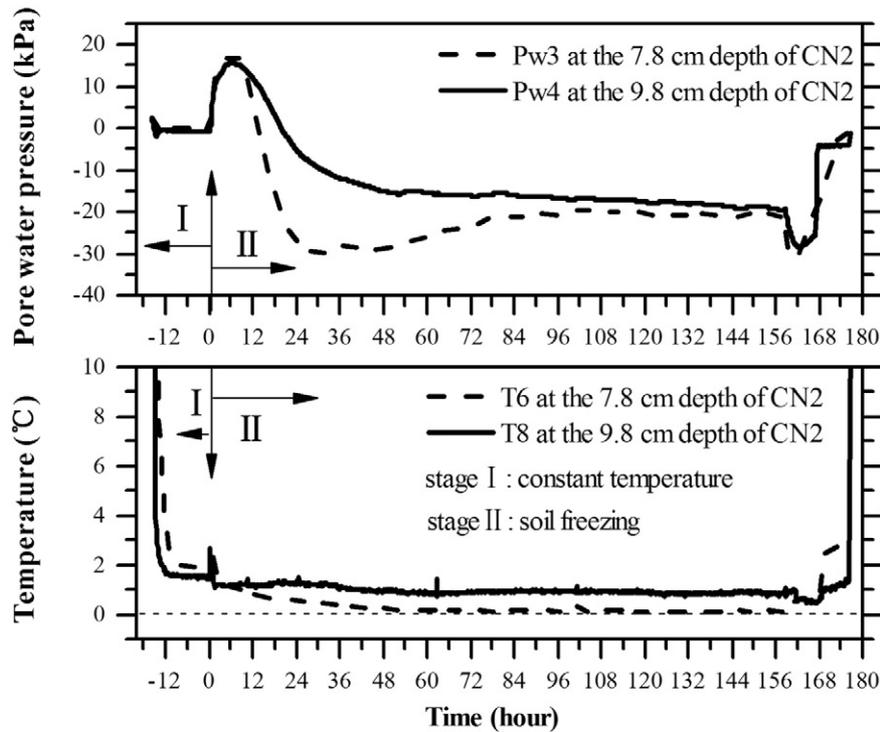

Fig. 7. Pore water pressure variations at different depths during the freezing of the CN2 sample.

heaving stress in the frozen fringe. During freezing, a significant increase in the frost heaving stress occurs that separates the soil particles during ice formation and segregation processes. Some studies indicated that increase in frost heaving stress results from increase in ice pressure (Gilpin, 1980; O'Neil and Miller, 1985). However, other studies, indicated that increase in frost heave stress results from the increase of thermo-molecular pressure due to the thinning of the premelted film between the solid ice and soil particles (Dash et al., 2006; Wettlaufer and GraeWorster, 2006). Although the surface of the soil sample was regarded as a free boundary without displacement constraints throughout soil freezing experiment, the soils in the frozen zone or frozen fringe could produce a frost heaving stress that was greater than the sum of the overburden soil weight and the external load (Fig. 8). This process was explained by the existence of soil tensile strength (Nixon, 1991) and by the frictional force between the frozen soil and the wall of the cylindrical Perspex cell (Smith and Onysko, 1990). The effects of frost heaving stress have rarely been considered in previous frost heave models. In these models, the differential equation for the total stress at equilibrium and at any time and point is presented as follows:

$$\frac{d\sigma}{dz} + \gamma = 0, \tag{1}$$

where σ is the total stress, z is the height, and γ is the unit weight of the soil. However, this equation is inappropriate if the effects of frost heaving stress are not considered, and considerable efforts have contributed to the measurement of frost heaving stress. The measured values were more than several dozen kilopascals greater than the values calculated by Eq. (1) during the ice-forming process (Akagawa et al., 2008; Smith and Onysko, 1990; Williams and Wood, 1985; Wood, 1990). Nixon (1991) first considered these excess values as the separation pressure and suggested that a new ice lens forms when the ice pressure equals or exceeds the sum of the overburden pressure and the separation pressure. Furthermore, based on the pore water pressure analysis in the previous section, the increase in pore water pressure during the early stage of freezing was controlled by the increase in the frost heaving stress. Herein, it is assumed that the frost heaving stress is mainly distributed in the frozen zone and frozen fringe (particularly in the frozen fringe), with no distribution in the unfrozen zone. When the pore water pressure and consolidation in the unfrozen zone are considered, the frost heaving stress in the frozen zone and frozen fringe can be reduced by varying the load $\sigma_f(z_f, t)$ at the freezing front. At the freezing front $x_f(t)$, the soil particles mainly bear the weight of the overburden frozen soil, the external load $P_l(t)$, and the frost heaving stress $\sigma_f(z_f, t)$. Therefore, the stress boundary conditions above the unfrozen zone can be expressed as follows:

$$\sigma\big|_{z=z_f(t)} = \int_{z_f(t)}^{H} \gamma dx + P_l(t) + \sigma_f(z_f(t)). \tag{2}$$

Frost heaving stress at the freezing front increases as the freezing front moves downward (Liu, 1981; Smith and Onysko, 1990). As shown in Fig. 9 (Fig. 4 in Smith and Onysko, 1990), when the soil temperature at some layer approaches a sub-freezing temperature Ts (Fig. 9a), the frost heaving stress is maximized along with ice formation and segregation (Fig. 9b). Next, the maximum frost heaving stresses at soil depths of 15 cm, 25 cm and 35 cm were extracted and plotted in Fig. 9c. The frost heaving stress in the freezing front is linearly related to the depth of the freezing front. Consequently, we assumed that

$$\sigma_f = A(H - z_f(t)). \tag{3}$$

Here, A is an empirical parameter with units of kPa/m (as shown in Table 3) and can be determined experimentally. The total stress at the freezing front can be obtained from equation (3) when the values of A and the freezing front coordinate z_f are known.

Accordingly, the total stress in the unfrozen zone can be presented as follows:

$$\sigma(z, t) = \int_{z}^{z_f(t)} \gamma dx + \int_{z_f(t)}^{H} \gamma dx + P_l(t) + \sigma_f(z_f, t). \tag{4}$$

The hydraulic boundary conditions at the freezing front involve changes in pore water pressure, which are controlled by thermodynamic processes in the frozen fringe. For saturated soils that are subjected to freezing, decrease in pore water pressure mainly results from negative temperature (Harlan, 1973). For unsaturated soils, decrease in pore water pressure mainly results from decrease in the degree of soil saturation (Sheng, 2011). For example, a larger pore water pressure decrease occurs when the initial moisture content is small (Fig. 6), and a smaller pore water pressure decrease occurs when the initial moisture content is large. Furthermore, based on the effective stress principle, change in pore water pressure is also induced by soil stress change (Chamberlain and Gow, 1979). For example, a significant increase in the pore water pressure occurs during the early stage of freezing (Figs. 4-7), which is mainly attributed to the pore compression that
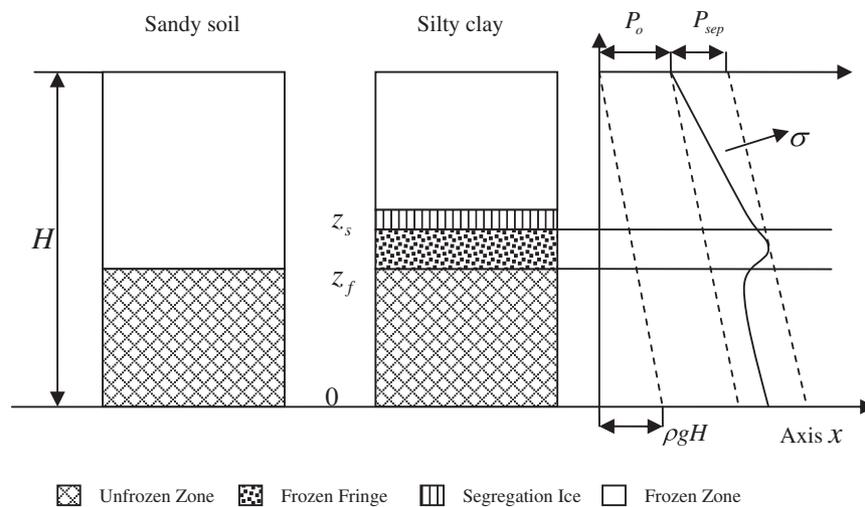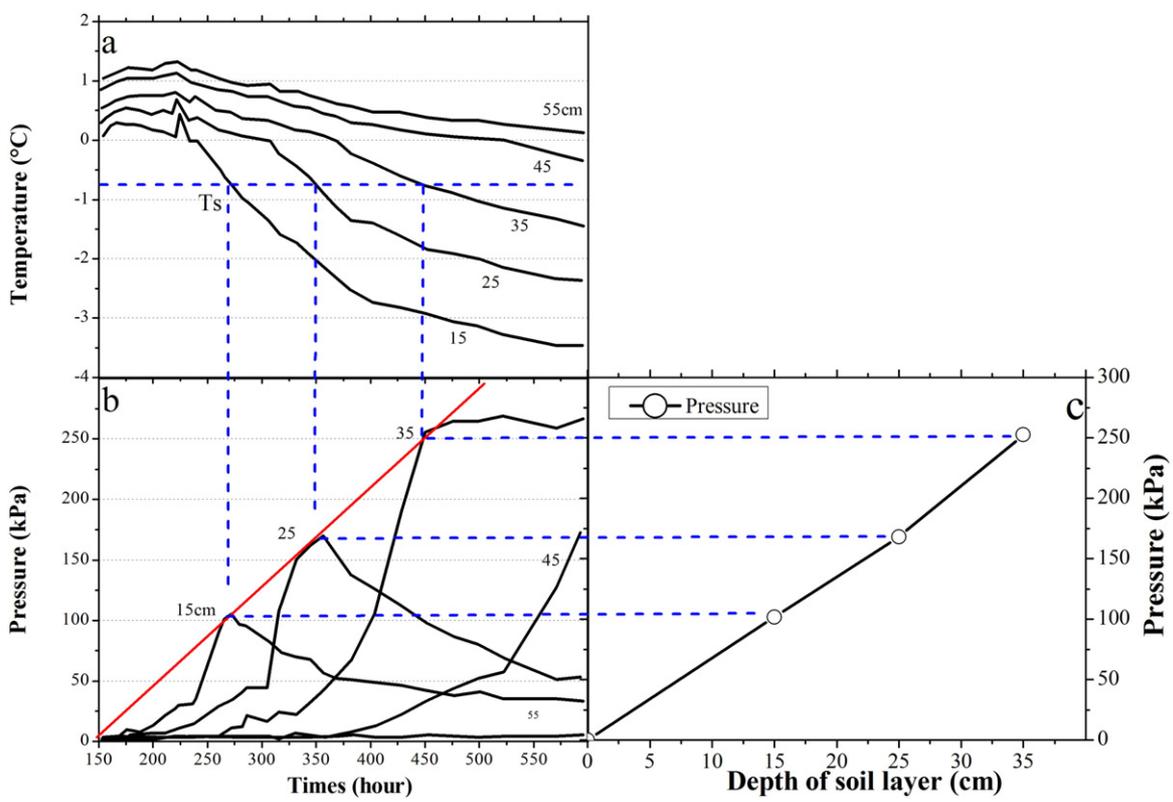

Fig. 8. Sketch of the zones and total stress during freezing of sandy soil and silty clay samples.

Fig. 9. Evolution of stress during freezing. (a) Variations of temperature over time at different depths, (b) variations of frost heaving stress over time at different depths, and (c) the dependency of the frost heaving stress on the soil layer depth.

results from an increase in frost heaving stress. Therefore, for unsaturated soils that are subjected to freezing, changes in pore water pressure can be attributed to the combined effects of sub-freezing temperature, the degree of saturation and soil stress. In addition, the solute concentration in the soil also induces a change in pore water pressure (Loch, 1978a, 1978b). Consequently, we assume that change in pore water pressure is controlled as follows:

$$\Delta P_{wf} = \Delta P_{wT} + \Delta P_{ww} + \Delta P_{wP} + \Delta P_{ws}. \tag{5}$$

where ΔP_{wf} is the total depression in pore water pressure; ΔP_{wT} is the depression in pore water pressure due to the temperature gradient when the soil sample is saturated; ΔP_{ww} is the depression in pore water pressure due to the degree of soil saturation; ΔP_{wP} is the depression in pore water pressure that is influenced by the internal stress changes of the soil (which involves external load and frost heaving stress changes); and ΔP_{ws} is the depression in pore water pressure due to the solute concentration.

In addition, the freezing rate is directly related to the decrease in pore water pressure at the freezing front. If the freezing rate is high, the freezing front advances quickly, and the pore water pressure decreases slightly. In contrast, if the freezing rate is slow, the freezing front advances slowly and the pore water pressure decreases significantly. Therefore, the relationship between pore water pressure and the depth of the freezing front is similar to the relationship between frost heaving stress and the depth of the freezing front, as shown in Fig. 9. Similarly, the pore water pressure in the freezing front above

the unfrozen zone can be reduced to a simple linear relationship as follows:

$$P_{wf} = B(H - z_f), \tag{6}$$

where B is an empirical parameter with units kPa/m (Table 3). Here, B can be determined experimentally. The pore water pressure at the freezing front can be obtained using Eq. (6) when B and the freezing front coordinate (z_f) are known.

As shown in Figs. 4–7, the pore water pressure in the unfrozen zone experiences a trend that increases first and decreases later. The observed increase in pore water pressure is mainly attributed to pore compression due to an increase in the frost heaving stress. In addition, the decrease in the pore water pressure is associated with the migration of water from the unfrozen zone to the frozen zone and frozen fringe. Thus, based on the pore water pressure analysis, we propose that consolidation of the unfrozen zone includes two components, compression-induced consolidation and vacuum-induced consolidation. Compression-induced consolidation results from an increase in frost heaving stress in the frozen fringe or external load. The compression-induced consolidation is dominant during the early stage of freezing because the stress is more quickly transferred by the effective force. Vacuum-induced consolidation results from a decrease in pore water pressure. The decrease in pore water pressure occurs in the later stage of freezing, and thus the vacuum-induced consolidation dominates the later stage of freezing.

Table 3
Parameters and values of simulation for silty clay soil tested.

Parameter	Value	Parameter	Value	Parameter	Value
A (kPa/m)	500	υ (1)	0.25	k_u (m/s)	1×10^{-10}
B (kPa/m)	-600	E (MPa)	13	k_f (m/s)	1×10^{-16}

In addition, previous studies showed that water expulsion during the early stage of freezing is commonly attributed to the volume change as water phases into ice (McRoberts and Morgenstern, 1975; Nakano, 1999). Herein, we propose that consolidation in the unfrozen zone is a significant factor for water expulsion based on the above analysis. Moreover, as shown in Fig. 6, soils with higher initial moisture contents have larger pore water pressure increases, and soils with lower initial moisture contents have smaller pore water pressure increases. This result indicates that water is more likely to be extruded from saturated soil during freezing.

3. Numerical simulation

3.1. Theoretical model for pore water pressure and consolidation phenomenon in the unfrozen zone

According to previous analyses, the changes in pore water pressure and consolidation phenomenon in the unfrozen zone was similar to those described by vacuum consolidation theory. Thus, we used vacuum consolidation theory as a reference to interpret the consolidation behavior in the unfrozen zone during freezing. Vacuum consolidation was commonly simulated by using Terzaghi's consolidation theory under a constant external load (Indraratna et al., 2005; Mohamedelhassan and Shang, 2002; Rujikiatkamjorn and Indraratna, 2007). However, the frost heaving stress during soil freezing varied with time. Therefore, consolidation in the unfrozen zone could be considered as vacuum-induced consolidation under time-dependent external loads. Here, we used Biot's consolidation theory to conduct a theoretical analysis and a numerical simulation, and the key was determining the boundary conditions at the freezing front.

The unfrozen zone in the z coordinate system is illustrated in Fig. 8. The bottom of the soil sample is located at $z = 0$, and the top of the soil sample is located at $z = H$, where H is the height of the soil sample. The freezing front is located at the coordinate point $z_f(t)$, which is a boundary that varies with time. During freezing, no frost heaving stress occurs in the unfrozen zone. Therefore, the differential equation of total stress at equilibrium and at any given time is

$$\nabla \cdot \sigma = \rho g. \tag{7}$$

Here, σ is the total stress tensor, ρ is the total density, and g is acceleration due to gravity. The governing equation for the flow field is derived from Darcy's law, and the continuity equation for moisture is as follows:

$$S_\alpha \frac{\partial P_w}{\partial t} + \nabla \cdot (-k\nabla P_w) = -\alpha_b \frac{\partial}{\partial t}(\nabla U). \tag{8}$$

Here, P_w is the pore water pressure, α_B is the Biot-Willis coefficient, S_α is the storage coefficient, and U is the displacement. The stress-strain relationships are defined as follows:

$$\begin{bmatrix} \sigma_x \\ \sigma_z \\ \sigma_{xz} \end{bmatrix} = \frac{E}{(1+v)(1-2v)} \begin{bmatrix} 1-v & v & 0 \\ v & 1-v & 0 \\ 0 & 0 & \frac{1-2v}{2} \end{bmatrix} \times \begin{bmatrix} \varepsilon_x \\ \varepsilon_z \\ \varepsilon_{xz} \end{bmatrix} - \begin{bmatrix} \alpha_B P_w & 0 & 0 \\ 0 & \alpha_B P_w & 0 \\ 0 & 0 & \alpha_B P_w \end{bmatrix}. \tag{9}$$

where E is the Young's modulus, v is Poisson's ratio, and the term $\alpha_B P_w$ is the contribution of the fluid pressure, which is often described as the fluid-to-structure coupling expression (Nasvi et al., 2014). The displacement-strain relationships are defined as follows:

$$\varepsilon_x = \frac{\partial u}{\partial x}, \varepsilon_z = \frac{\partial v}{\partial z}, \varepsilon_{xz} = \frac{1}{2}\left(\frac{\partial u}{\partial z} + \frac{\partial v}{\partial x}\right), \varepsilon_{xz} = \varepsilon_{zx}. \tag{10}$$

By inserting Eqs. (8) and (9) into Eq. (7), the governing equation for stress equilibrium with the displacement variable can be obtained as follows:

$$\frac{E}{2(1+v)}\nabla^2 U + \frac{E}{2(1+v)(1-2v)}\nabla(\nabla \cdot U) = \alpha_b P_w. \tag{11}$$

In summary, the Biot consolidation theory under time-dependent external loading in the unfrozen zone is composed of Eqs. (7), (8), (9) and (10).

3.2. Case analysis

The size of the unfrozen zone varies with time as the freezing front advances downward. This process is viewed as a moving boundary problem and can be simulated using the arbitrary Lagrangian-Eulerian (ALE) method in COMSOL (Carin, 2006). Furthermore, the simulation must determine the variations in the stress and pore water pressure at the freezing front, while the boundary at the bottom of the soil sample is generally used to distinguish between open-system and closed-system conditions. This simulation can reflect the changing trends of pore water pressure that are affected by various factors.

3.2.1. Case A: the closed-system condition
Case A involved the freezing of CN2 saturated silty clay soil sample under closed-system condition. In this case, the height of the soil sample was 13.3 cm; the top, bottle and box temperatures were −8 °C, 3 °C and 1 °C, respectively; and the sidewall of the cell was insulated. The freezing front gradually advanced downward and then remained stable at a height of 5.5 cm when a constant temperature was applied at the top of the soil sample. The stress boundary and hydraulic boundary conditions at the freezing front were based on Eqs. (2) and (6). Because the soil sample was saturated and under no external load, the total stress and pore water pressure were approximated and reduced to simple linear relationships, as shown in Eqs. (12) and (13), regardless of the self-weight of the soil sample.

$$\sigma\Big|_{z=z_f(t)} = \sigma_f(z_f(t)) \approx A(H-z_f) \tag{12}$$

$$P_w(z_f, t) = P_{wT} \approx B(H-z_f) \tag{13}$$

The evolution of the freezing front was obtained by fitting the temperature data in the CN2 experiment, as shown in Fig. 10a. Fig. 10c shows the variations of the total stress and pore water pressure at the freezing front with time based on Eqs. (12) and (13). The hydraulic boundary at the bottom of the soil sample in the closed-system condition was presented as follows:

$$k_u \frac{\partial P_w}{\partial z}\Big|_{z=0} = 0, \tag{14}$$

where k_u is the hydraulic conductivity of the unfrozen zone; the other parameters used in the simulation are shown in Table 3. Parameter A was obtained by referring to the pressures shown in Fig. 9. As shown in Fig. 9c, the slope of the internal stress with depth was approximately 650 kPa/m. Thus, we assumed that this parameter was approximately 500 kPa/m. Similarly, parameter B was obtained from the pore water pressure measured in our study. As shown in Fig. 6, the maximum decrease of the pore water pressure in the saturated soil was approximately 35 kPa, and the depth of the freezing front was approximately 6 cm. Therefore, the slope of the pore water pressure with depth was approximately −600 kPa/m. However, the v, E, k_u and k_f parameters were all obtained from papers that investigated similar soils (Yang et al., 2008; Wen et al., 2011; Zhou and Li, 2012). Our calculations indicated that the simulated Pw3 and Pw4 pore water pressures fit the measured Pw3 and Pw4 pore water pressure data well (Fig. 11).

3.2.2. Case B: the open-system condition

This case investigated CN1 saturated silty clay soil sample under open-system conditions. The height of the soil sample was 12.5 cm; the top, bottle and box temperatures were −5 °C, 1 °C and 1.5 °C, respectively; and the sidewall of the cell was insulated. The freezing front gradually advanced downward and then stabilized at a height of 6.3 cm when a constant temperature was applied at the top of the soil sample. The stress boundary and the hydraulic boundary conditions at the freezing front under open-system condition were also represented by Eqs. (12) and (13), which were similar to the closed-system conditions presented in Section 3.2.1 (Fig. 10d). The evolution of the freezing front with time was plotted in Fig. 10b. The hydraulic boundary at the bottom of the soil sample under the open-system condition was presented as follows:

$$P_w|_{z=0} = 0. \tag{15}$$

The parameters required for the simulation can be found in Table 3. According to our calculation, the simulated pore water pressure fit the measured Pw3 pore water pressure data well (Fig. 12).

The uplift of the soil surface during freezing is the sum of the frost heave in the frozen zone and consolidation in the unfrozen zone. However, in previous numerical simulations and in the analysis of data from unidirectional freezing tests, the uplift of the soil surface has always been reduced to the frost heave in the frozen zone without considering consolidation in the unfrozen zone. Therefore, greater uplift is always obtained from the simulation relative to the measured value at the soil surface. Herein, the importance of consolidation is acknowledged. Thus, the consolidation behavior and boundary conditions of the unfrozen zone were interpreted in detail with regard to pore water pressure

variations, which were expected to promote the theoretical development of an accurate frost heave model. In the early stage of freezing, some water is extruded from the saturated soil samples as the pore water pressure increases. This process implies that the unfrozen zone experiences an apparent compression-induced consolidation process. However, the pore water pressure significantly decreased during the later stages of freezing in the closed-system experiments. This finding implies that the unfrozen zone experiences a vacuum-induced consolidation process. Notably, deformation of the unfrozen zone depends not only on consolidation process but on swelling process. For example, some water will be absorbed into the unfrozen zone in the open-system condition because suction occurs. Therefore, the unfrozen zone may experience an apparent swelling process that is accompanied by increase of moisture content. The relationships regarding the deformation of the unfrozen zone are considered an aspect of unsaturated soil research. Herein, we did not conduct the further investigations that are referred to by Sheng (2011).

4. Conclusions

This study of the pore water pressures in the unfrozen zone during unidirectional freezing tests in the laboratory has yielded the following conclusions:

1) Temperature changes over a range of positive temperatures do not result in pore water pressure changes in the unfrozen zone. In addition, the pore water pressure in the unfrozen zone generally increases at first and then decreases. Changes in the pore water pressure in the unfrozen zone are mainly controlled by stress and hydraulic boundary conditions. Furthermore, changes in pore water pressure are affected by soil type, water supply condition, initial soil moisture content,
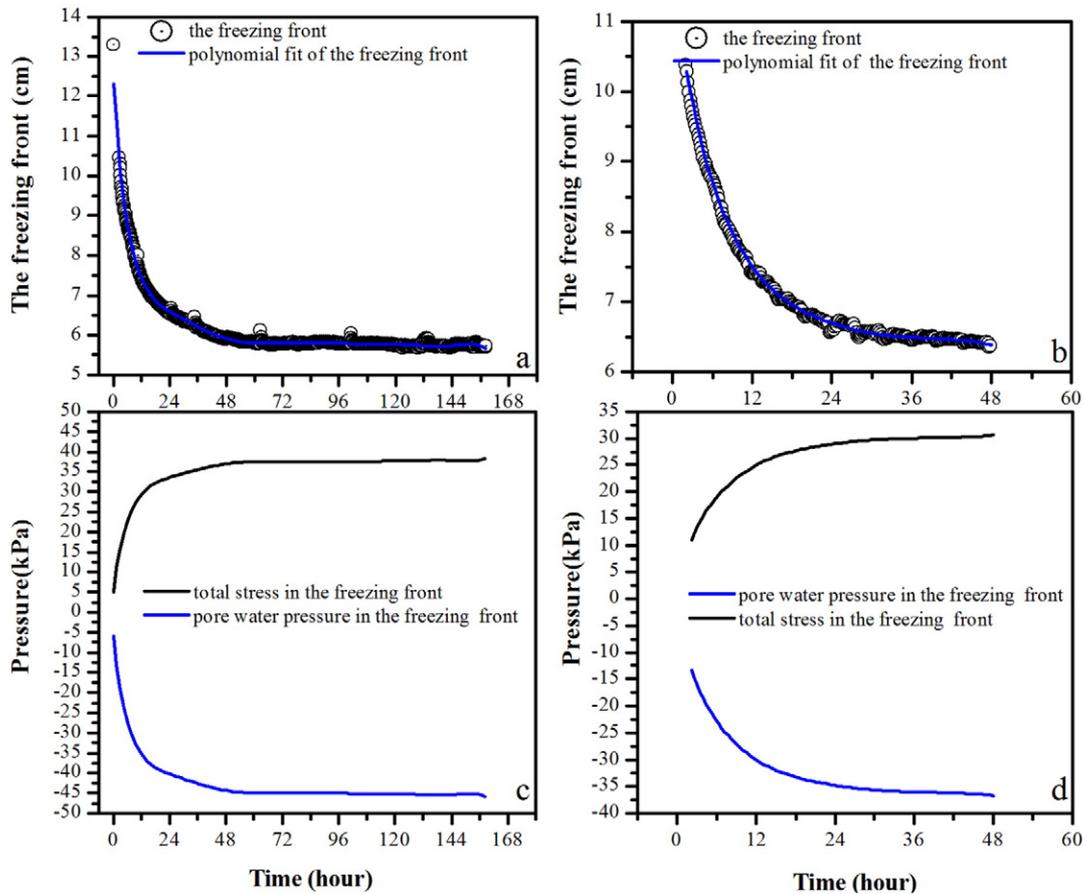

Fig. 10. The boundary conditions in the freezing front, including the (a) evolution of the freezing front during experiment CN2, (b) evolution of the freezing front during experiment CN1, (c) total stress and pore water pressure at the freezing front with time during experiment CN2, and (d) the total stress and pore water pressure in the freezing front with time during experiment CN1.
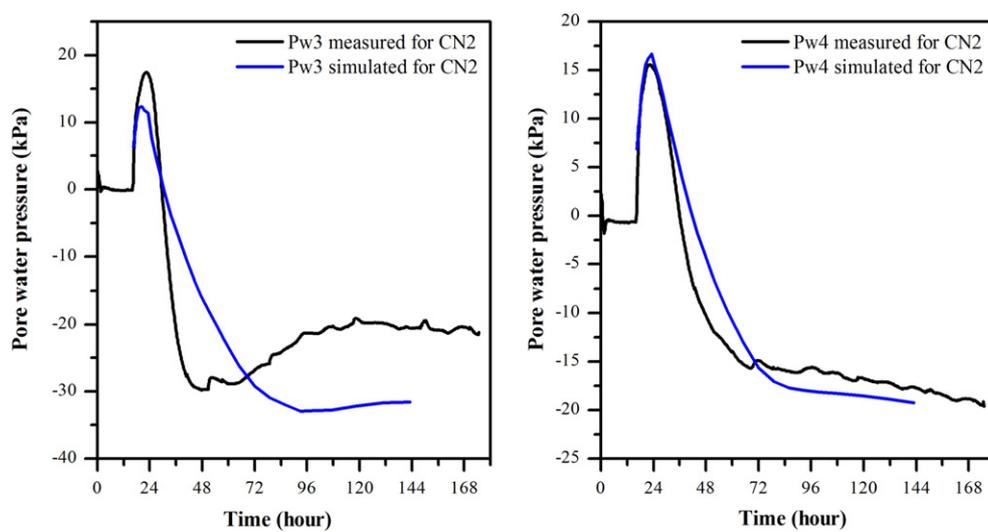
Fig. 11. Comparison of the measured and simulated pore water pressures in the unfrozen zone during closed-system freezing of CN2.

measured soil layer depth, and hydraulic conductivity. Conversely, changes in the pore water pressure in the unfrozen zone indicated an increase in the frost heaving pressure and a decrease in the pore water pressure at the freezing front and the frozen fringe during freezing.

2) Based on the changes of the pore water pressure in the unfrozen zone, we propose that consolidation in the unfrozen zone during freezing results from compression-induced and vacuum-induced consolidation. Different consolidation patterns are responsible for different stages of freezing. Compression-induced consolidation primarily occurs during the early stage of soil freezing as the pore water pressure increases, and vacuum-induced consolidation mainly occurs during the later stage of soil freezing as the pore water pressure decreases.

3) Water extrusion is commonly viewed as an increase in volume that results from the transformation of water into ice. Furthermore, consolidation in the unfrozen zone is a significant factor that induces water extrusion. During the early stage of soil freezing, water was extruded because of the pore water pressure increases due to the compression-induced consolidation of the unfrozen zone. During the later stage of soil freezing, water was absorbed into the frozen zone and the frozen

fringe because the pore water pressure decreased, which resulted in vacuum-induced consolidation of the unfrozen zone.

4) In addition, the uplift of the soil surface during freezing is attributed to the combined effects of frost heave deformation in the frozen zone and consolidation deformation in the unfrozen zone. The importance of consolidation is realized from the variations of the pore water pressure that were observed in this paper. Therefore, consolidation deformation in the unfrozen zone should be considered for accurate frost heave modeling.

References

Akagawa, S., Hiasa, S., Kanie, S., et al., 2008. Pore water and effective pressure in the frozen fringe during soil freezing. Proceedings of the Ninth International Conference on Permafrost. 1, pp. 13–18.
Arenson, L.U., Xia, D., Sego, D., et al., 2005. Brine and unfrozen water migration during the freezing of Devon silt. Proceedings of the Fourth Biennial Workshop on Assessment and Remediation of Contaminated Sites in Arctic and Cold Climates, pp. 35–44.
Bronfenbrener, L., 2013. Non-equilibrium crystallization in freezing porous media: numerical solution. Cold Reg. Sci. Technol. 85, 137–149.
Carin, M., 2006. Numerical simulation of moving boundary problems with an ALE method. Validation in the case of a free surface or a moving solidification front. Comsol Multiphysics Conference, pp. 219–224.
Chamberlain, E.J., 1981. Overconsolidation effects of ground freezing. Eng. Geol. 18, 97–110.
Chamberlain, E.J., Gow, A.J., 1979. Effect of freezing and thawing on the permeability and structure of soils. Eng. Geol. 13 (1–4), 73–92.
Dash, J., Rempel, A., Wettlaufer, J.S., 2006. The physics of premelted ice and its geophysical consequences. Rev. Mod. Phys. 78 (3), 695–741.
Eigenbrod, K.D., Knutsson, S., Sheng, D.C., 1996. Pore-water pressures in freezing and thawing fine-grained soils. J. Cold Reg. Eng. 10 (2), 77–92.
Fukuda, M., 1983. The pore water pressure profile in porous rocks during freezing. Proceedings of the Fourth International Conference on Permafrost. 1, pp. 322–327.
Gilpin, R.R., 1980. A model for the prediction of ice lensing and frost heave in soils. Water Resour. Res. 16 (5), 918–930.
Harlan, R.L., 1973. Analysis of coupled heat-fluid transport in partially frozen soil. Water Resour. Res. 9 (5), 1314–1323.

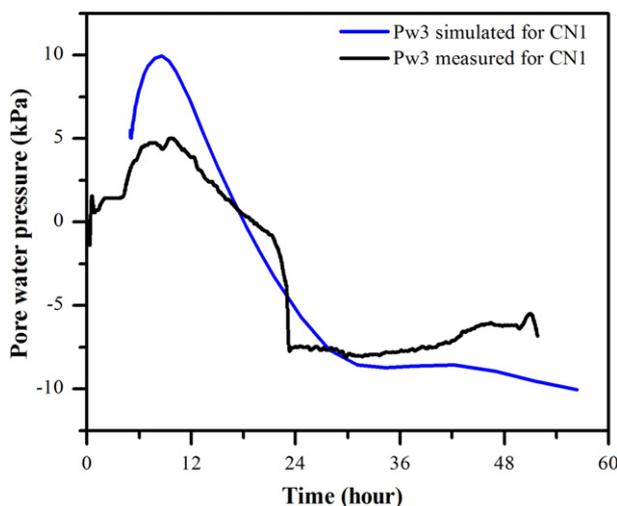**Fig. 12.** Comparison of the measured and simulated pore water pressures in the unfrozen zone during open-system freezing of CN1.

Harris, C., Davies, M.C.R., 1998. Pore-water pressures recorded during laboratory freezing and thawing of a natural silt-rich soil. Proceedings 6th International Conference on Permafrost. 1, pp. 433–440.

Indraratna, B., Rujikiatkamjorn, C., Sathananthan, I., 2005. Analytical and numerical solutions for a single vertical drain including the effects of vacuum preloading. Can. Geotech. J. 42 (4), 994–1014.

Konrad, J.M., Morgenstem, N.R., 1980. A mechanistic theory of ice formation in fine grained soils. Can. Geotech. J. 17, 473–486.

Konrad, J.M., Morgenstem, N.R., 1981. The segregation potential of a freezing soil. Can. Geotech. J. 18, 482–491.

Liu, H., 1981. On calculation of normal frost heaving force. J. Glaciol. Geocryol. 3 (2), 13–17 in Chinese.

Liu, J., Shen, Y., Zhao, S., 2011. High-precision thermistor temperature sensor: technological improvement and application. J. Glaciol. Geocryol. 33 (4), 765–771 in Chinese.

Loch, J.P.G., 1978a. Water redistribution in partially frozen, saturated silt under several temperature gradients and overburden loads. Soil Sci. Soc. Am. J. 42 (3), 400–406.

Loch, J.P.G., 1978b. Thermodynamic equilibrium between ice and water in porous media. Soil Sci. 126 (2), 77–80.

Ma, W., Zhang, L., Yang, C., 2015. Discussion on applicability of the generalized Clausius-Clapeyron equation and the frozen fringe process. Earth Sci. Rev. 142 (2015), 47–59.

Mcgaw, R.W., Berg, R.L., Ingersoll, J.W., 1983. An investigation of transient processes in an advancing zone of freezing. Proceedings of 4th International Conference on Permafrost, pp. 821–825.

McRoberts, E.C., Morgenstern, N.R., 1975. Pore water expulsion during freezing. Can. Geotech. J. 12 (1), 130–141.

Miller, R.D., 1978. Frost heaving in non-colloidal soils. Proceedings 3th International Conference on Permafrost. 1, pp. 708–713.

Mohamedelhassan, E., Shang, J.Q., 2002. Vacuum and surcharge combined one-dimensional consolidation of clay soils. Can. Geotech. J. 39 (5), 1126–1138.

Nakano, Y., 1999. Water expulsion during soil freezing described by a mathematical model called M1. Cold Reg. Sci. Technol. 29, 9–30.

Nasvi, M.C.M., Ranjith, P.G., Sanjayan, J.A., 2014. Numerical study of CO_2 flow through geopolymer under down-hole stress conditions: application for CO_2 sequestration wells. J. Unconv. Oil Gas Resour. 7, 62–70.

Nixon, J.F., 1991. Discrete ice lens theory for frost heave in soils. Can. Geotech. J. 28 (6), 843–859.

O'Neil, K., Miller, R.D., 1985. Exploration of a rigid ice model of frost heave. Water Resour. Res. 21 (3), 281–296.

O'neill, K., 1983. The physics of mathematical frost heave models: a review. Cold Reg. Sci. Technol. 6 (3), 275–291.

Penner, E., 1970. Frost heaving forces in leda clay. Can. Geotech. J. 7 (1), 8–16.

Rujikiatkamjorn, C., Indraratna, B., 2007. Analytical solutions and design curves for vacuum-assisted consolidation with both vertical and horizontal drainage. Can. Geotech. J. 44 (2), 188–200.

Sheng, D., 2011. Review of fundamental principles in modelling unsaturated soil behaviour. Comput. Geotech. 38 (6), 757–776.

Smith, M.W., Onysko, D., 1990. Observations and significance of internal pressures in freezing soil. Proceedings of the Fifth Canadian Permafrost Conference 54. Nordicana, Laval, pp. 75–82.

Takagi, S., 1980. The adsorption force theory of frost heaving. Cold Reg. Sci. Technol. 3, 57–81.

Takashi, T., Ohrai, T., Yamamoto, H., et al., 1981. Upper limit of heaving pressure derived by pore-water pressure measurement of partially frozen soil. Eng. Geol. 18, 245–257.

Thomas, H.R., Cleall, P., Li, Y.C., et al., 2009. Modelling of cryogenic processes in permafrost and seasonally frozen soils. Géotechnique 59 (3), 173–184.

Tiedje, E.W., Guo, P., 2011. Dewatering induced by frost heave in a closed system. Pan-Am CGS Geotechnical Conference http://geoserver.ing.puc.cl/info/conferences/PanAm2011/panam2011/pdfs/GEO11Paper559.pdf.

Watanabe, K., 2008. Water and heat flow in a directionally frozen silty soil. Proceedings of the Third Hydrus Workshop, pp. 15–22.

Wen, Z., Ma, W., Feng, W., et al., 2011. Experimental study on unfrozen water content and soil matric potential of Qinghai-Tibetan silty clay. Environ. Earth Sci. 66 (5), 1467–1476.

Wettlaufer, J.S., GraeWorster, M., 2006. Premelting dynamics. Annu. Rev. Fluid Mech. 38 (4), 27–52.

Williams, P.J., Wood, D.J.A., 1985. Internal stresses in frozen ground. Can. Geotech. J. 22, 413–416.

Wood, J.A., 1990. The role of irreversible thermodynamics and rheology in the regelation-flow phenomenon. Cold Reg. Sci. Technol. 18, 133–145.

Yang, C., He, P., Cheng, G., et al., 2008. Study of stress-strain relationships and strength characteristics of saturated saline frozen silty clay. Rock Soil Mech. 29 (12), 3282–3286.

Zhang, L., Ma, W., Yang, C., et al., 2013. A review and prospect of the thermodynamics of soil subjected to freezing and thawing. J. Glaciol. Geocryol. 35 (6), 1505–1518.

Zhang, L., Ma, W., Yang, C., et al., 2014. Investigation of the pore water pressures of coarse-grained sandy soil during open-system step-freezing and thawing tests. Eng. Geol. 181 (2014), 233–248.

Zhang, L., Ma, W., Yang, C., et al., 2015. Pore water pressure changes of supercooling and ice nucleation stages during freezing point testing. Geotech. Lett. 5, 39–42.

Zhou, J., Li, D., 2012. Numerical analysis of coupled water, heat and stress in saturated freezing soil. Cold Reg. Sci. Technol. 72, 43–49.